Chemical Engineering Journal 452 (2023) 139197

Contents lists available at ScienceDirect

Chemical Engineering Journal

journal homepage: www.elsevier.com/locate/cej

Tailored design of highly permeable polyamide-based nanofiltration membrane via a complex-dissociation regulated interfacial polymerization

Yufan Hao [1], Na Yang [1], Longfei Zhang, Yao Fang, Yongli Sun, Bin Jiang, Luhong Zhang *

School of Chemical Engineering and Technology, Tianjin University, Tianjin 300072, People's Republic of China

ARTICLE INFO

Keywords:
Nanofiltration
Polyamide
Interfacial polymerization
Complex
Dissociation

ABSTRACT

Nanofiltration (NF) that can separate neutral/charged solutes is considered as a key industrial technology in water softening and wastewater treatment. However, commercial polyamide (PA) NF membranes, with undesirable surface properties and excessive mass transfer resistance, seriously restrict the permeability and are easily attached by pollutants. In this study, a novel complex-dissociation regulated interfacial polymerization (CDRIP) strategy was proposed to prepare highly permeable polyamide-based (PA-based) NF membranes, in which tannic acid (TA)/Ca(II) complex was *in situ* formed on substrate surface and then dissociated by sodium citrate (SC) after interfacial polymerization. Interestingly, SC can not only adjust surface properties of PA, such as hydrophilicity and surface charge, but also form water-soluble SC/Ca(II) complexes for constructing additional transport channels within the separation layer to reduce mass transfer resistance. After the dissociation of TA/Ca(II) complex, TA remained on the membrane surface to further regulate the surface properties of separation layer. The results showed that the PA/TA/Ca(II)-SC NF membrane maintained a high Na_2SO_4 rejection (98.5 %) and a remarkable water permeability of 31.7 $L{\cdot}m^{-2}{\cdot}h^{-1}{\cdot}bar^{-1}$, which is 2-fold that of the pristine PA NF membrane. Moreover, the prepared NF membrane exhibits favorable operation stability and anti-fouling ability. Therefore, by employing the CDRIP method, the permeability of NF membrane can be further improved almost without sacrificing the rejection of Na_2SO_4, which provides a green and efficient strategy for the fabrication of high-performance PA-based NF membranes.

1. Introduction

Membrane separation technology, as a key industrial technology, is attracting emerging interests in alleviating global energy/environmental crisis [1,2]. Nanofiltration (NF) membrane has been increasingly explored in wastewater treatment, water softening and water purification by virtue of its size sieving and charge repulsion [3,4]. Among these applications, the removal of Na_2SO_4 with NF membranes is being widely used to avoid health hazards in drinking water and prevent scaling in industrial equipment [5,6]. The most common commercially available NF membranes are polyamide (PA) prepared by interfacial polymerization. However, it presents a huge challenge to further enhance the water permeance of NF membranes while retaining admirable selectively rejection of target solute. Unfortunately, there are two factors that severely restrict the improvement of membrane permeability. One is the undesirable surface properties of PA membrane, such as the weak surface hydrophilicity and the less surface charge, which are not strong enough to attract water molecules and repulsive to charged solutes [7,8]. The other is the dense crosslinked structure and excessive mass transfer resistance of PA, which hinders the rapid permeation of water molecules. Therefore, it is indispensable to develop efficient strategies to prepare high-permeability NF membranes through focusing on both membrane structure and surface properties to achieve sustainable task-specific separation.

In recent years, many researchers focused on surface modification technologies relying on the active groups (residual acyl chloride groups, carboxyl groups and amide bonds) on the surface of PA membrane [3]. Most commonly, some hydrophilic materials, such as amines [9–11], ionic liquids [7,12], alcohols [13,14] and zwitterions [15,16], are grafted onto PA membrane through covalent bonds. Although the permeability of membrane can be improved to varying degrees by the above hydrophilic modification methods, it is still limited by the mass transfer resistance of the intrinsic PA membrane structure. In order to reduce mass transfer resistance, many strategies, such as reducing

* Corresponding author.
E-mail address: zhanglvh@tju.edu.cn (L. Zhang).
[1] These authors contribute equally to this work.

https://doi.org/10.1016/j.cej.2022.139197
Received 5 July 2022; Received in revised form 28 August 2022; Accepted 9 September 2022
Available online 17 September 2022

thickness [17,18], constructing extra water transport channels [19,20], and increasing effective permeable area [21,22] of the PA layer, have shown positive signs in improving the permeability of NF membrane. Considering that the ultra-thin PA membranes possess high permeability but are easily damaged, the construction of extra transport channels within the PA layer may present extraordinary potential in facilitating the rapid passage of solvents. In general, the incorporation of porous/embedded nanomaterials could provide the internal channels of nanomaterial or the external channels between nanomaterial and PA matrix, inducing the transport of solvents through the preferential channels [23]. Although various applications of porous materials have been developed and shown potential in water remediation [24–26]. However, there are still some obstacles to the introduction of nanomaterials, such as poor compatibility [23], potential leaching [27] and nanomaterial toxicity [28].

Tannic acid (TA), a kind of plant polyphenol, contains catechol active groups, which can not only coordinate with metal ions [29,30], but also interact with the membrane through covalent or non-covalent bonds [31,32], thus it is considered as a promising natural material for membrane modification. For instance, Guo et al. prepared separation layers of polyamide/polyester/chelate structure by interfacial polymerization with the assistance of TA and Fe^{3+}, and then soaked the membrane in NaOH solution for etching polyester structure to obtain loose NF membranes [33]. It's worth noting that the mass transfer resistance of the separation layer decreased greatly after etching polyester structure, accompanied by the phenomenon that TA can still regulate the properties of the membrane, such as enhancing the interface interaction between substrate and separation layer. Therefore, instead of etching the polyester, we hypothesized that the dissociation of chelate structure can also reduce the mass transfer resistance of the separation layer by constructing transport channels. Meanwhile, TA remained on the membrane after the dissociation of TA complex may continue to act on the PA membrane. Sodium citrate (SC), as a hydroxyl carboxylate, has strong metal coordination ability [34] and high hydrophilicity [35]. Recently, researchers have gradually noticed that the hydrophilicity of SC/citric acid can be used in the surface modification of membranes [35,36]. Furthermore, the SC/Ca(II) complexes are water-soluble, exhibiting great potential in building transport channels inside the membrane. However, to the best of our knowledge, the application of SC as a strong organic ligand to dissociate metal complexes has not been reported for membrane modification.

Herein, we propose a complex-dissociation regulated interfacial polymerization (CDRIP) strategy that TA/Ca(II) complex was *in situ* formed on the surface of polyacrylonitrile (PAN) ultrafiltration membranes and then dissociated by SC after interfacial polymerization for the preparation of highly permeable PA/TA/Ca(II)-SC NF membranes. The dissociation of TA/Ca(II) complexes directly reduces the mass transfer resistance of membrane, and forms additional transport channels to promote the preferential transport of solutes. Besides, some surface properties of PA/TA/Ca(II)-SC NF membranes, mainly including hydrophilicity and surface charge, were enhanced by SC and TA. Furthermore, the separation performance of NF membrane was investigated by changing the content of Ca^{2+}, the concentration and the post-treatment time of SC. Moreover, the operation stability and antifouling performance of the prepared NF membrane were evaluated. The aim of this work is to elucidate the influences of the TA/Ca(II) complex dissociated by SC on the structure and surface properties of PA-based NF membrane, as well as the relationship between membrane structure-surface properties-separation performance.

2. Experimental

2.1. Materials and chemicals

Commercial polyacrylonitrile (PAN, Mw = 150 kDa) ultrafiltration membranes were supplied by Shandong Megavision Membrane Technology Engineering Co., ltd. Sodium acetate (1 M, pH = 5) and Tris (hydroxymethyl)-aminomethane (Tris-HCl, 1 M, pH = 8.5) buffers were purchased from Senbeijia Biological Technology Co., ltd. Tannic acid (TA, AR), Piperazine (PIP, 99 %, AR) and trimesoyl chloride (TMC, 99 %, AR) were provided from Aladdin Chemical Co. ltd. Sodium citrate (SC, 98 %, AR) and Bovine serum albumin (BSA, 98 %, AR) were bought from Shanghai Macklin Biochemical Technology Co., ltd. Various inorganic salts (Na_2SO_4, $MgSO_4{\cdot}7H_2O$, $MgCl_2{\cdot}6H_2O$, NaCl and $CaCl_2$, AR) and *n*-hexane (AR) were obtained from Tianjin Kemiou Chemical Reagent Co. ltd. Diethylene glycol (DEG, 106 Da) and polyethylene glycol (PEG) of different molecular weights (200, 400, 600 and 1000 Da) were bought from Sinopharm Chemical Reagent Co., ltd. All of the chemical materials were used directly without further purification.

2.2. Pretreatment of substrate

Prior to interfacial polymerization, the polyacrylonitrile (PAN) substrates were immersed in deionized water for about 12 h. Next, 0.1 g tannic acid (TA) powder was dissolved in 100 mL Tris-HCl buffer solution (50 mM, pH = 8.5) to prepare 1 mg/mL TA solution. Then, the PAN substrate was wiped off and fixed on a fixture. Immediately, the TA solution was poured onto the top surface of PAN substrate and then put the fixture with a fixed shaking rate of 60 rpm at room temperature. After 1 h, the soaked PAN substrate was cleaned twice with deionized water and heated for 10 min in an oven at 60 °C. For clarity, the PAN substrate pretreated by TA is named PAN-TA substrate.

2.3. Interfacial polymerization and post-treatment

The preparation process of PA/TA/Ca(II)-SC NF membrane is shown in Fig. 1. 0.05 g anhydrous calcium chloride ($CaCl_2$) and 0.25 g piperazine (PIP) were dissolved successively in 99.7 g sodium acetate buffer solution (50 mM, pH = 5) to prepare aqueous phase solution. The organic phase solution containing 0.1 wt% trimesoyl chloride (TMC) was prepared by dissolving 0.1 g TMC into 99.9 g *n*-hexane. In this case, the aqueous phase solution was soaked on the upper surface of the substrate and stood for 30 min. Then, the aqueous phase solution was poured out, and the membrane was dried at room temperature to obtain the PAN-TA-(PIP-$CaCl_2$) substrate. After that, the organic phase solution was poured onto the PAN-TA-(PIP-$CaCl_2$) substrate for 30 s. The membrane was immediately transferred to an oven at 60 °C for 5 min to make the reaction more complete and to remove the residual *n*-hexane. After heating, the membrane was immersed in 1 wt% sodium citrate (SC) solution for post-treatment, and then stored in deionized water for reserve. The membrane is labelled as PA/TA/Ca(II)-SC NF membrane. As a supplement, the content of Ca^{2+} (0–0.1 wt%), the concentration (0–10 wt%) and post-treatment time (1–12 h) of SC were optimized, respectively. On the contrary, after heating, the membrane without SC post-treatment was retained in deionized water to remove incomplete acyl chloride, which is referred as PA/TA/Ca(II) NF membrane. For comparison, the traditional polyamide (PA) NF membrane was obtained by PIP and TMC interfacial polymerization without $CaCl_2$ under the same conditions, which is denoted as PA NF membrane. In addition, the PA NF membrane was immersed in SC solution to obtain PA-SC NF membrane.

2.4. Characterization methods

In order to investigate the interaction between Ca^{2+}, TA and SC, the characteristic peaks of TA in three solutions (TA, TA-Ca^{2+} and TA-Ca^{2+}-SC) were measured using a UV–vis spectrometer (UV-4802S, Unico, US). The surface chemical compositions of membranes were characterized by Attenuated total reflectance-Fourier transform infrared spectroscopy (ATR-FTIR, Nicolet 6700, US) and X-ray photoelectron spectra (XPS, Thermo Scientific K-Alpha, US). The morphologies of the membranes were measured using a scanning electron microscopy (SEM, Hitachi,

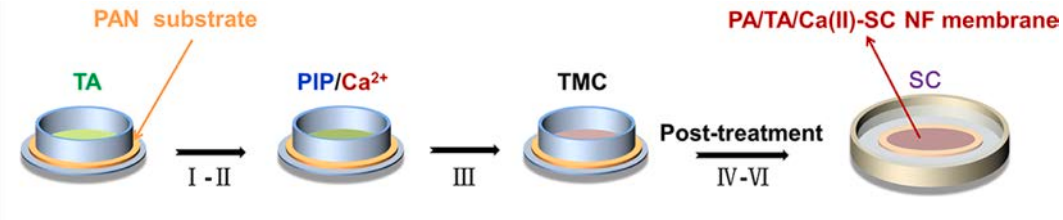

Fig. 1. Schematic illustration of the fabrication process of PA/TA/Ca(II)-SC NF membrane.

Regulus 8100, Japan). The cross-sectional morphologies of the NF membranes were further observed by a transmission electron microscope (TEM, JEM-1400Flash, Japan) at an accelerated voltage of 80 kV after the membrane being treated by ultrathin section specimens. Surface morphologies and roughness of the membranes were observed by atomic force microscopy (AFM, Bruker Dimension Icon, USA) in ScanAsyst mode. The surface hydrophilicity of membrane was visualized on a contact angle meter (JC 2000 goniometer, Powereach, China). The surface charge on membrane was collected from a SurPASS electrokinetic analyzer (Anton Paar, USA) at the pH about 7. The organic carbon contents of feed and permeate solutions, respectively, were measured using a total organic carbon instrument (TOC, Shimadzu, Japan).

2.5. Separation performance test

The separation performance of the prepared NF membranes was evaluated by the cross-flow mode with a 7.1 cm^2 effective membrane area. Each membrane samples were prepressed at a pressure of 6 bar for 0.5 h and held at a steady pressure of 5 bar for 0.25 h before the membrane test. The feed concentration of inorganic salt (Na_2SO_4, $MgSO_4$, $MgCl_2$ or NaCl) was 1000 ppm.

The water flux (J, $L{\cdot}m^{-2}{\cdot}h^{-1}$) was determined by the following Eq. (1):

$$J = (\Delta V)/(A{\cdot}\Delta t) \tag{1}$$

where ΔV is the permeate water volume (L), Δt is the permeation time (h), and A represents the effective filtration area (m^2).

The water permeance ($L{\cdot}m^{-2}{\cdot}h^{-1}{\cdot}bar^{-1}$) was calculated as follows:

$$Permeance = J/(\Delta P) \tag{2}$$

where ΔP is the operating pressure (bar).

The solute rejection was determined by the following Eq. (3):

$$R\ (\%)\ = (C_f - C_P)/C_f \times 100\% \tag{3}$$

where C_f and C_p, measured by a conductivity monitor (DDS-307A, Shanghai Leici, China), represent the concentrations of salt in the feed solute and permeate solute respectively.

2.6. Determination of membrane pore size and distribution

The pore size of NF membrane was determined by filtration of 200 ppm neutral molecule, including diethylene glycol (DEG, 106 Da) and a series of polyethylene glycol (PEG) molecules (molecular weights of 200, 400, 600 and 1000 Da) [37]. The DEG and PEG concentrations were calculated from the contents of total organic carbon (TOC). The molecular weight cut-off (MWCO) is the molecular weight of the neutral molecule at a rejection rate of 90 %. The Stokes radius of neutral molecule can be calculated by the following Eq. (4) [38]:

$$r_p = 16.73 \times 10^{-12} \times M^{0.557} \tag{4}$$

where M is the molecular weight of neutral molecule, and r_p is the Stokes radius.

The average pore radius and distribution of the NF membrane were obtained based on a log normal probability function between the rejection of solute and r_p [39]. The pore radius distribution curve can be expressed following the relationship [12]:

$$\frac{dR(r_p)}{dr_p} = \frac{1}{r_p \ln\sigma_p \sqrt{2\pi}} \exp\left[-\frac{\left(\ln r_p - \ln\mu_p\right)^2}{2\left(\ln\sigma_p\right)^2} \right] \tag{5}$$

where r_p is the pore radius of the NF membrane, μ_p is the geometric mean radius of the neutral solute when R is 50 %. The σ_p is the geometric standard deviation of μ_p, which is the ratio of neutral solute radius when R is 84.13 % and 50 % [40].

2.7. Repeatability evaluation

The repeatability of the NF membranes was measured by filtration pure water and Na_2SO_4 solution (1000 ppm) at 5 bar, respectively. A filtration cycle was defined as follows: 30 min filtration for pure water, 30 min filtration for Na_2SO_4 solution and 10 min of physical cleaning with pure water. The repeatability of the membranes was assessed for 5 cycles.

2.8. Antifouling properties evaluation

In order to ensure that the NF membranes can be tested under the same conditions of lateral hydrodynamic characteristics, the initial pure water flux of different membranes was consistent by controlling the operating pressure before the antifouling experiment [41,42]. The antifouling performance of the NF membranes was explored as follows: firstly, pure water as the feed solution was filtrated the membranes for 3 h and then the feed solution was changed to bovine serum albumin (BSA) for another 7 h. Next, the feed solution was replaced by pure water and the contaminants on the membrane were removed through physical cleaning without applied pressure. The flux recovery ratio (FRR) and the flux decline ratio (FDR) was calculated as follows [43,44]:

$$FRR\ (\%)\ = J_c/J_0 \times 100\% \tag{6}$$

$$FDR\ (\%) = (J_0 - J_s)/J_0 \times 100\% \tag{7}$$

where J_0 is the initial flux, J_c is the water flux after washing and J_s is the steady flux after fouling.

3. Results and discussion

3.1. Design of the PA/TA/Ca(II)-SC NF membranes

At the beginning, we analyzed the interaction between Ca^{2+}, TA and SC in solution by the intensity variation of TA characteristic peaks in UV–vis absorption spectra (Fig. S1). After the introduction of Ca^{2+}, the intensity of TA characteristic peak (275 nm) decreased sharply, corresponding to the lightening of the TA-Ca^{2+} solution color and the emergence of flocculation at the bottom, confirming the formation of TA/Ca (II) complex. This phenomenon is attributed to the fact that TA can coordinate with Ca^{2+} to form stable ring chelates under alkaline conditions by the deprotonated phenolic hydroxyl groups [45–47]. It is

similar to the coordination behavior of most phenolic compounds with Ca^{2+}. For example, phenolic compounds such as guaiacol and eugenol have been extracted by complexation precipitation with Ca^{2+} [48,49]. Interestingly, the intensity of TA characteristic peak almost returned to its original value after being poured into SC solution, accompanied by the dissolution of flocculation and the restoration of solution color. It indicates that SC can dissociate the coordination bond in TA/Ca(II) complex to form a more stable and water-soluble SC/Ca(II) complex. It provides a new perspective for constructing transport channels in the separation layer of NF membrane. Based on this, a novel CDRIP strategy was proposed to prepare highly permeable PA/TA/Ca(II)-SC NF membrane. We speculated that the TA/Ca(II) complexes mainly existed between PA and the substrate, and then dissociated by SC after interfacial polymerization to reduce the mass transfer resistance of membranes. And beyond that, it is also expected that SC and TA can improve the surface properties of PA.

3.2. Membrane characterizations

Before coating the organic phase solution, the functional groups of the substrate were analyzed by ATR-FTIR spectra in Fig. S2. PAN-TA-(PIP-$CaCl_2$) substrate showed a new characteristic peak at 1573 cm^{-1} (-C═N) and a weakened characteristic peak at 3419 cm^{-1} (–OH), indicating that TA was involved in Michael addition reaction with PIP [50] and also in coordination with Ca^{2+} [30]. On this basis, the surface chemical structures of the substrate and all the prepared NF membranes were characterized by ATR-FTIR spectra, as shown in Fig. 2a. Compared with PAN substrate, all NF membranes showed new peak at about 1622–1627 cm^{-1}, respectively, due to the stretching vibration of C═O (amide I band) in PA, proving that PA was successfully formed on the surface of the NF membranes [51].

To further study the influence of SC post-treatment on membrane surface chemistry, the elemental compositions of NF membranes were investigated by XPS. In Table 1 and Fig. 2b, Na content of PA-SC NF membrane is 0.28 %, which proves that SC can be anchored on the PA membrane surface. This is because hydroxyl groups on SC molecules can react with residual acyl chloride groups on TMC molecules to form ester bonds, which has been reported in the literature [43,52]. At the same time, SC may wash away part of PA oligomers with high carboxylic acid content, resulting in a decrease of O element content from 14.74 % to 13.83 % [36]. In addition, the presence of TA/Ca(II) complex on the surface of PA/TA/Ca(II) NF membrane was demonstrated, because Ca element (0.80 %) was observed and O content increased from 14.74 % to 19.21 % for the contribution of TA. After SC post-treatment, no Ca element was detected in PA/TA/Ca(II)-SC NF membrane, suggesting that the complex of TA/Ca(II) on the membrane surface was dissociated by SC. Furthermore, EDS characterization of the membrane was carried out, and the results showed that no obvious Ca signal was found (Fig. S3), indicating that Ca^{2+} was completely released from the PA/TA/Ca(II)-SC NF membrane. Moreover, Na element (0.65 %) was detected on its surface, while the O content increased from 19.21 % to 20.62 % when compared with PA/TA/Ca(II) NF membrane. We believe that the dissociation of the TA/Ca(II) complex on the membrane surface exposes more acyl chloride groups and promotes the anchoring of SC. Fig. 2c–f represents the O 1 s high resolution spectra of the prepared NF membrane, in which the two peaks at 531.1 eV and 532.7 eV are attributed to *N*-C═O*/O-C═O* and O═C-O* bonds, respectively [53,54]. For PA-SC NF membrane, the ratio of O═C-O* bond decreases from 19.67 % to 15.69 % after SC post-treatment, confirming that SC indeed washed away part of PA oligomers. Compared with PA NF membrane, the O═C-O*/C—O*-R bond ratio of PA/TA/Ca(II) membrane increases from 19.67 % to 34.36 %, which is contributed to the presence of C—O*-R in TA/Ca(II) complex on the membrane surface. After SC post-treatment,

Table 1
The elemental compositions of the membranes characterized with XPS.

Sample	C (%)	O (%)	N (%)	Na (%)	Ca (%)
PA	75.08	14.74	10.18	–	–
PA-SC	75.70	13.83	10.19	0.28	–
PA/TA/Ca(II)	70.63	19.21	9.36	–	0.80
PA/TA/Ca(II)-SC	70.15	20.62	8.58	0.65	–

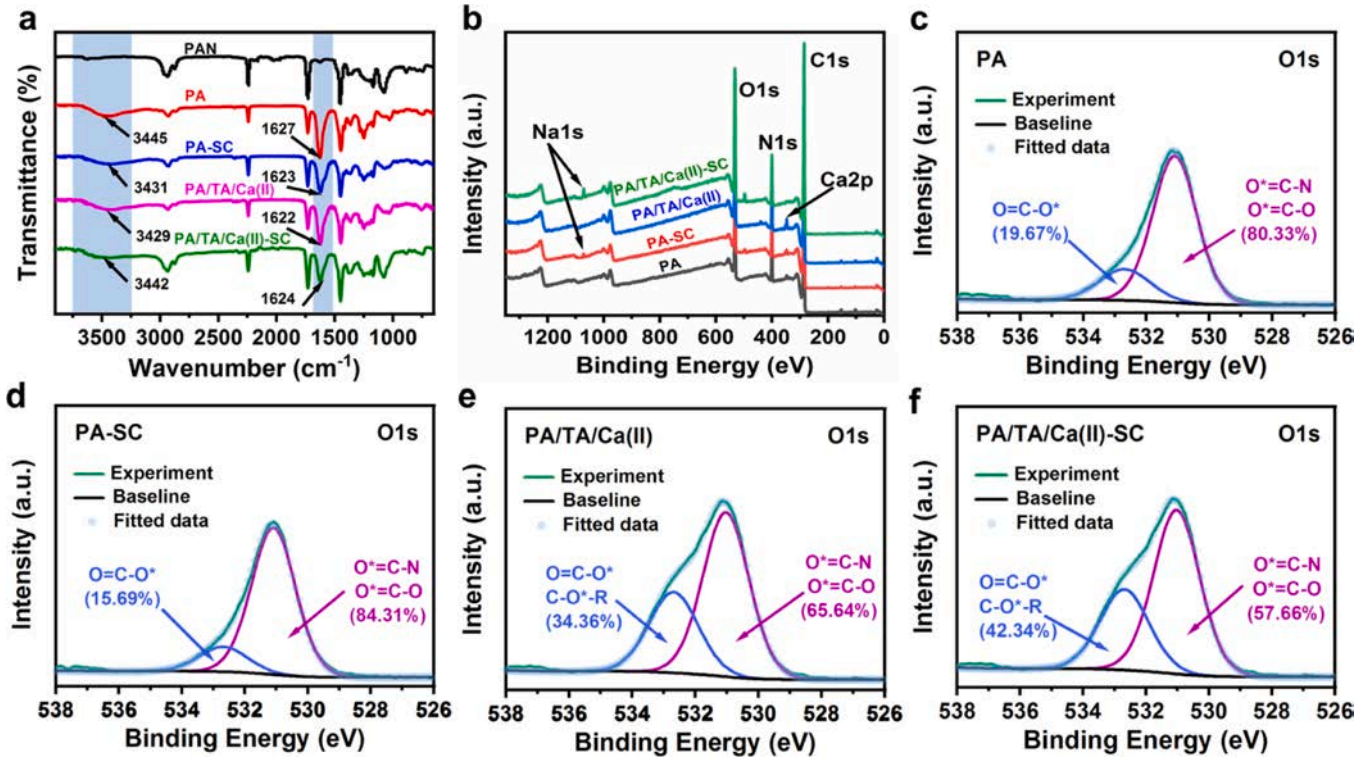

Fig. 2. (a) ATR-FTIR spectra, (b) XPS full scale spectrum and (c-f) O 1 s high resolution spectra of the NF membranes.

the ratio of O═C-O*/C—O*-R bond in PA/TA/Ca(II)-SC NF membrane increased from 34.36 % to 42.34 %, corresponding to more SC on the membrane surface.

The surface morphologies and roughness of NF membranes were studied by SEM and AFM, respectively, as shown in Fig. 3. Normally, traditional nodular structures appeared on the surface of PA and PA-SC NF membranes, and the average surface roughness (Ra) of PA-SC NF membrane increased slightly from 3.9 nm to 4.9 nm. However, the nodular structures were distributed in different sizes and the Ra of PA/TA/Ca(II) NF membrane increased from 3.9 nm to 6.1 nm, which is related to the influence of TA/Ca(II) complex on the formation of PA. The presence of TA/Ca(II) complex can be proved by SEM to characterize the surface and cross section morphology of the substrate (Fig. S4), and the color change of the substrate can be observed (Fig. S5). After SC post-treatment, PA/TA/Ca(II)-SC membrane exhibited a larger nodular structure with a corresponding increases in Ra from 6.1 nm to 11.4 nm, which may be attributed to the fluctuation of the separation layer caused by the dissociation of TA/Ca(II) complex.

Fig. 4 shows the cross-sectional structures of NF membranes observed by SEM and TEM, respectively. For PA-SC NF membrane, the thickness of separation layer is about 75 ± 4 nm, slightly thinner than PA NF membrane (80 ± 5 nm). For PA/TA/Ca(II) NF membrane, some large nodular structures are visible on its surface by reason of the TA/Ca (II) complex on the substrate surface. Besides, the separation layer thickness of PA/TA/Ca(II) membrane (58 ± 8 nm) is thinner than that of PA membrane (80 ± 5 nm), mainly because the introduction of TA increases the hydrophilicity of the substrate and promotes the uniform dispersion of PIP, and the Michael addition of TA and PIP impedes the diffusion of PIP and slows down the interfacial polymerization [55–57]. For PA/TA/Ca(II)-SC membrane, notably, hollow structures appear mostly between the separation layer and the substrate and partly in the PA. It can be explained by the dissociation of the water-insoluble TA/Ca (II) complex to form the water-soluble SC/Ca(II) complex, and the partial space occupied by the original TA/Ca(II) complex is vacated. The dissociation of TA/Ca(II) complexes mainly existing between PA and substrate will directly reduce the mass transfer resistance of the membrane, while the dissociation of partially dispersed complexes in PA layer will form additional transport channels to promote solute preferential transport, which is considered beneficial to the improvement of water permeability. Furthermore, the hollow structure also increases the effective permeable area of the membrane and has been reported to facilitate the penetration of water molecules [58]. Moreover, the thickness of the separation layer (50 ± 6 nm) is thinner than PA/TA/Ca (II) NF membrane, which is considered to be the shedding of PA oligomers on the surface.

The hydrophilicity and surface zeta potential of the NF membranes were characterized to investigate the influence of SC post-treatment on membrane surface properties, as shown in Fig. 5a and b. Compared with PA NF membrane, PA-SC NF membrane displays smaller water contact angle (47.3°) and more negative surface zeta potential (-44.6 mV) at pH = 7.0, indicating SC molecules anchored on the membrane surface can enhance the hydrophilicity and surface negative charge of the membrane, because the ionization degree of SC is higher than that of carboxylic acid [35]. For PA/TA/Ca(II) NF membrane, the water contact angle (54.4°) is similar to that of PA NF membrane, but the surface zeta potential is more negative (-47.5 mV) than that of PA NF membrane (-42.4 mV). It corresponds to the situation that TA exists on the membrane surface in the form of TA/Ca(II) complex, which can not significantly upgrade the surface hydrophilicity of the membrane. But the phenolic hydroxyl groups on TA after deprotonation can enhance the electronegativity of the membrane [54,59]. However, compared with PA/TA/Ca(II) NF membrane, the water contact angle of PA/TA/Ca(II)-SC NF membrane decreased from 54.4° to 43°, even lower than that of PA-SC NF membrane. This can be explained by the synergistic effect of two factors: more hydrophilic groups of TA are exposed after the dissociation of Ca^{2+} and more SC molecules anchored on the membrane surface, which comprehensively improves the hydrophilicity of the membrane. Besides, the surface zeta potential of PA/TA/Ca(II)-SC NF membrane (-45.9 mV) is less negative than that of PA/TA/Ca(II) NF membrane. The reason for this phenomenon is that some TA may fall off from the membrane accompanied by the dissociation of Ca^{2+}, reducing the content of charged groups on the membrane surface. Notably, the characteristic peak of TA (275 nm) in SC solution after soaking PA/TA/Ca(II) NF membrane was detected by UV–vis absorption spectra (Fig. S6). Furthermore, the surface zeta potential of PA/TA/Ca(II)-SC NF membrane is more negative than PA and PA-SC NF membrane caused by the presence of TA and SC on the membrane surface, which will enhance the rejection of negatively charged solutes. Moreover, it can be seen that all the NF membranes are negatively charged in the pH range of 4–10. When the pH value is less than 5, the amounts of amino groups remaining on the membrane before and after SC post-treatment should be the same, resulting in similar charge properties. With the increase of pH, the ionization of carboxylic acid is enhanced, showing stronger electronegativity, which is beneficial to improve the rejection of divalent anions. When the pH value is greater than 6, the ionization of carboxylic acid is basically completed, and the charge property of membrane tends to be stable, which is consistent with the literature [12].

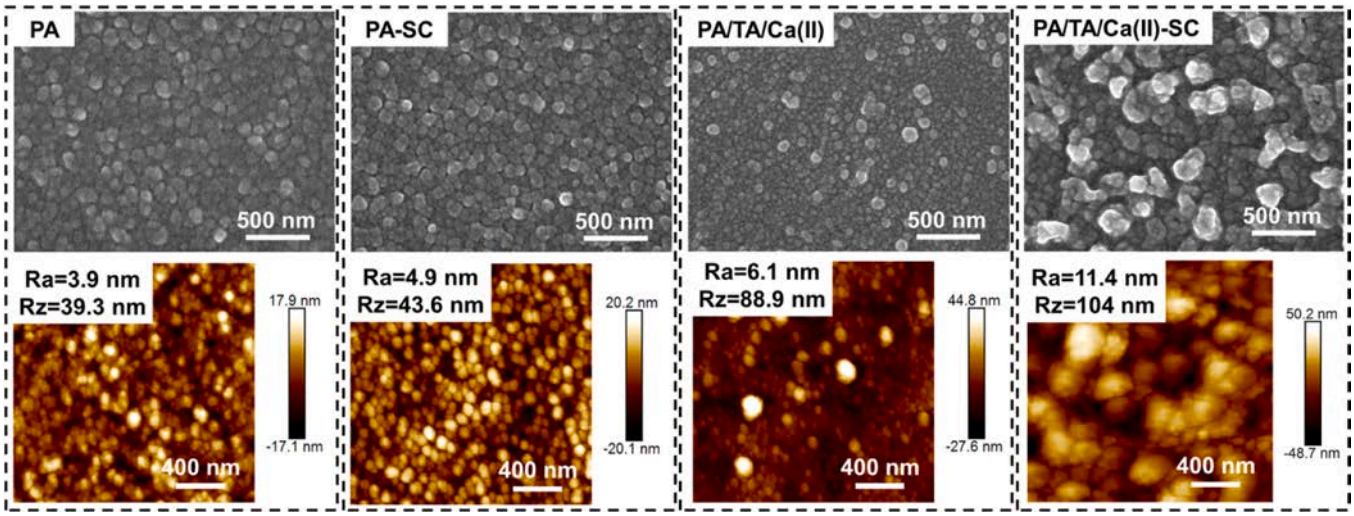

Fig. 3. SEM and AFM surface morphologies of the NF membranes.

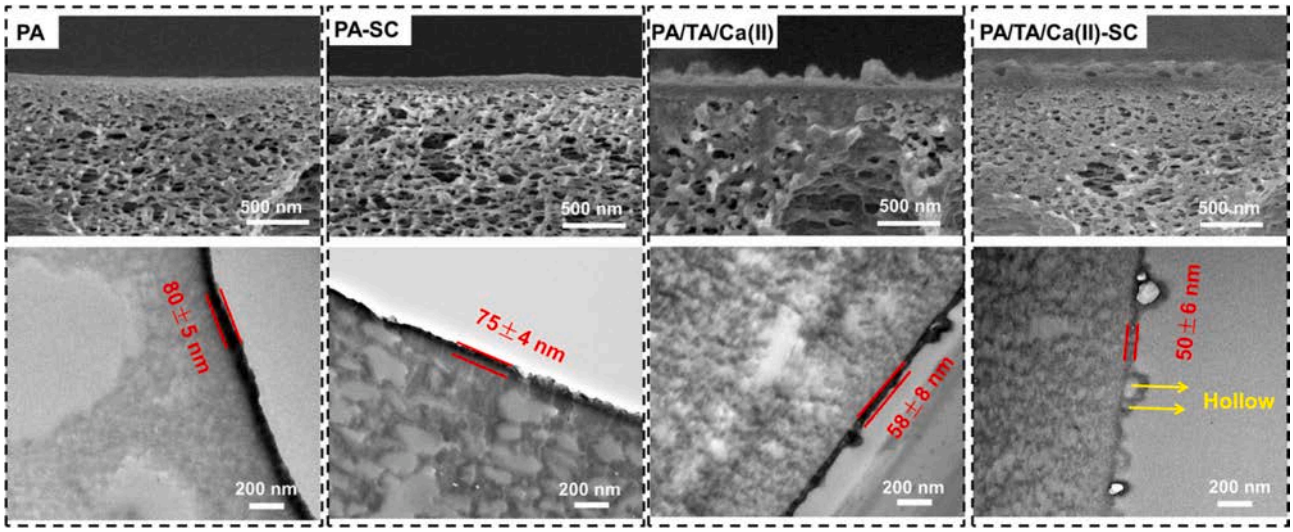

Fig. 4. SEM and TEM cross-sectional morphologies of the NF membranes.

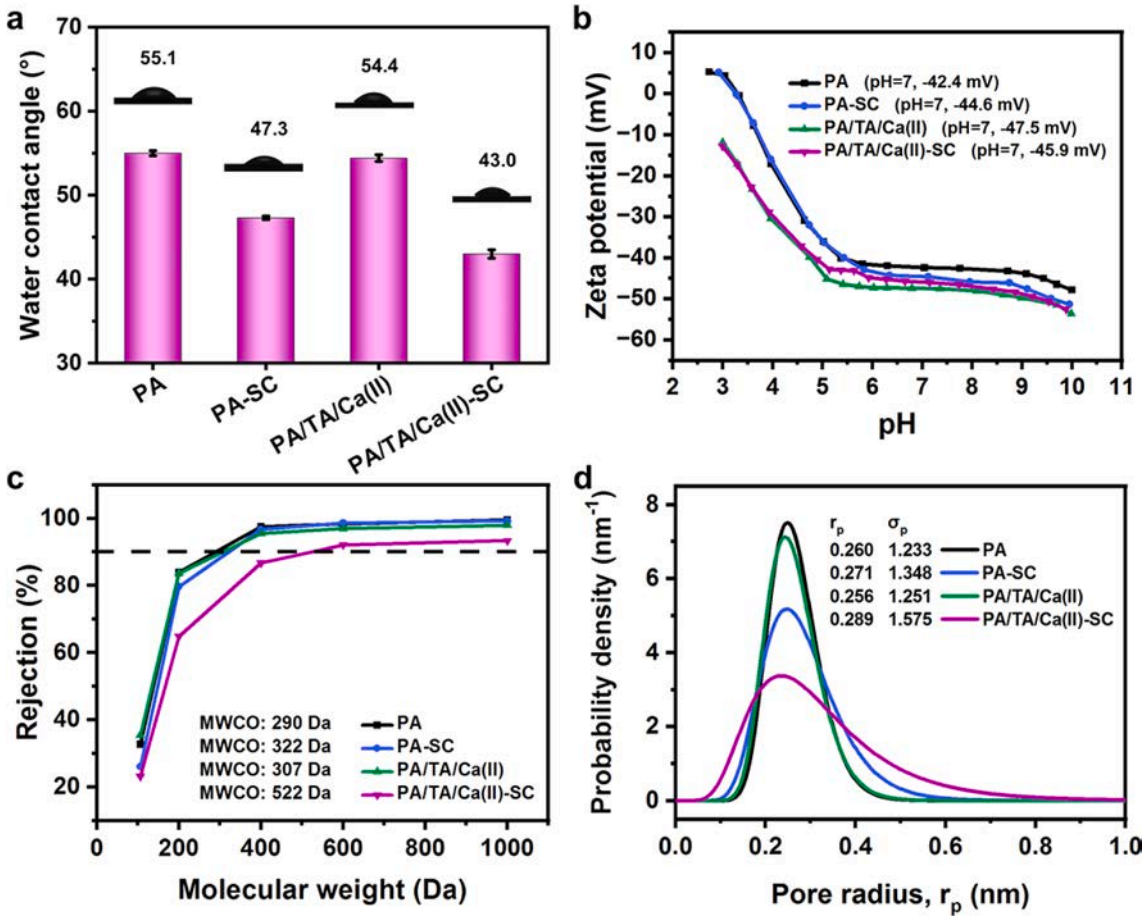

Fig. 5. (a) Static water contact angles, (b) surface zeta potential (examined with 0.01 M KCl solution), (c) rejection curves to DEG and PEG with different molecular weight and (d) surface pore radius distribution of the NF membranes.

In order to explore the pore structure of membrane, the molecular weight cut-off (MWCO) of NF membranes were tested by intercepting DEG and PEG of different molecular weights, as shown in Fig. 5c. Compared with PA NF membrane, the MWCO of PA-SC NF membrane increased from 290 Da to 322 Da, which corresponded to a mean pore radius of about 0.27 nm (Fig. 5d) [60]. Besides, the MWCO of PA/TA/Ca (II) NF membrane is 307 Da, yielding mean pore radius of 0.26 nm, which is close to that of PA NF membrane. In particular, the MWCO of PA/TA/Ca(II)-SC NF membrane is increased to 522 Da, and its mean pore radius is about 0.29 nm. Furthermore, the pore radius distribution of PA/TA/Ca(II)-SC NF membranes is wider (Fig. 5d). This phenomenon can be interpreted as that the dissociation of Ca^{2+} constructs additional channels in the separation layer of PA/TA/Ca(II)-SC NF membrane, which may promote the solute transport.

3.3. Desalination performance of PA/TA/Ca(II)-SC NF membranes

The pure water flux and the rejection rate of Na_2SO_4 (1000 ppm) of the NF membranes were characterized as shown in Fig. 6a. Compared with PA NF membrane, the pure water flux of PA-SC NF membrane is slightly increased from 15.9 $L{\cdot}m^{-2}{\cdot}h^{-1}{\cdot}bar^{-1}$ to 19.1 $L{\cdot}m^{-2}{\cdot}h^{-1}{\cdot}bar^{-1}$, and the Na_2SO_4 rejection is reduced from 99.6 % to 99.2 %, revealing that SC can slightly improve the permeability of the membrane (about 20 %). Besides, for PA/TA/Ca(II) NF membrane, the pure water flux is about 12.0 $L{\cdot}m^{-2}{\cdot}h^{-1}{\cdot}bar^{-1}$, which is lower than that of PA NF membrane, and the rejection rate of Na_2SO_4 is about 99.7 %. However, the pure water flux of PA/TA/Ca(II)-SC NF membrane is significantly increased to 31.7 $L{\cdot}m^{-2}{\cdot}h^{-1}{\cdot}bar^{-1}$, which is equivalent to 2.6 times that of PA/TA/Ca(II) NF membrane. It is noteworthy that the permeation flux of PA/TA/Ca(II)-SC NF membrane is 2-fold of PA NF membrane, proving that this CDRIP strategy can significantly improve the membrane permeability. Combined with the reaction mechanisms and structure models of membranes (Figs. S7–S9), it is considered that the two factors act together to obtain high permeability by this CDRIP strategy. First and foremost, the dissociation of TA/Ca(II) complex directly reduces the mass transfer resistance and promotes the rapid transport of water molecules, which includes the construction of additional transport channels and the expansion of pore size [57,61]. Secondly, the improvement of surface hydrophilicity benefited from the anchoring of SC also facilitates the transport of water molecules [35]. Meanwhile, the rejection rate of PA/TA/Ca(II)-SC NF membrane to Na_2SO_4 is still up to 98.5 %, which is determined by the synergistic effect of size sieving and Donnan exclusion. In order to explain this phenomenon, the schematic illustration of separation mechanism is complemented in Fig. S10 of the supporting information, reflecting that the enhancement of membrane surface negative charge plays an important role in partially offset the rejection loss caused by pore size expansion.

Besides, the effect of Ca^{2+} concentration on the separation performance was discussed in Fig. 6b, since the content of Ca^{2+} was considered to be directly related to the degree of complexation and dissociation of TA/Ca(II). The pure water flux of PA/TA/Ca(II)-SC NF membrane kept increasing from 11.3 $L{\cdot}m^{-2}{\cdot}h^{-1}{\cdot}bar^{-1}$ to 52.6 $L{\cdot}m^{-2}{\cdot}h^{-1}{\cdot}bar^{-1}$ when the content of Ca^{2+} increased from 0 wt% to 0.1 wt%. Unfortunately, the rejection rate of Na_2SO_4 declined to 95.7 % when the content of Ca^{2+} reached 0.1 wt%. It can be explained that excessive Ca^{2+} not only participated in the formation of TA/Ca(II) complex, but also promoted the hydrolysis of TMC and formed loose PA membrane, which has been reported by previous studies [62,63]. Therefore, the concentration and soaking time of SC solution were further investigated when the content of Ca^{2+} was controlled at 0.05 wt%. Next, the influence of SC concentration on the separation performance was explored in Fig. 6c. With the increase of SC solution concentration, the pure water flux of the PA/TA/Ca(II)-SC NF membrane showed an upward trend. However, when SC concentration continued to increase to 10 wt%, the rejection rate of Na_2SO_4 decreased sharply, so that 1 wt% SC concentration was selected to further analyze the influence of SC post-treatment time on the separation performance as shown in Fig. 6d. With the increase of SC post-treatment time from 1 h to 12 h, the pure water flux of the PA/TA/Ca(II)-SC NF membrane tended to be stable when it reached 6 h, indicating that the TA/Ca(II) complex was basically dissociated at this time.

Fig. 7a and b display the salt flux and salt rejection of PA and PA/TA/Ca(II)-SC NF membrane for different inorganic salt solutions. It can be seen that the Na_2SO_4 flux of PA/TA/Ca(II)-SC NF membrane is 24.7 $L{\cdot}m^{-2}{\cdot}h^{-1}{\cdot}bar^{-1}$, far higher than PA NF membrane (11.7 $L{\cdot}m^{-2}{\cdot}h^{-1}{\cdot}bar^{-1}$), and the fluxes of the other three salts keep a similar trend. For PA NF membrane, the salt rejection follows the order of Na_2SO_4 (99.6 %) > $MgSO_4$ (97.7 %) > $MgCl_2$ (50.3 %) > NaCl (41.7 %),

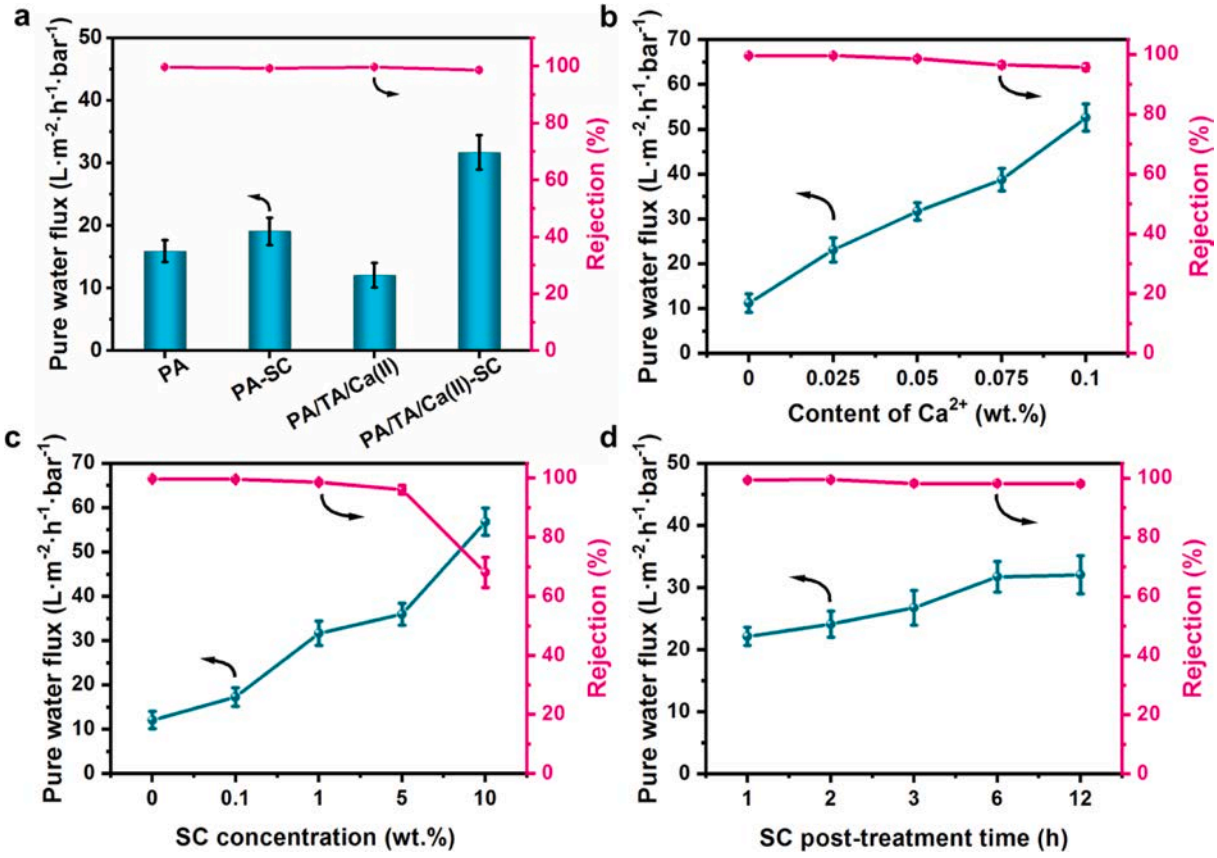

Fig. 6. Separation performance of the membranes. (a) The pure water flux and the rejection of Na_2SO_4 of NF membranes. (b-d) The effects of Ca^{2+} content, SC concentration and SC post-treatment time on the filtration performance of the PA/TA/Ca(II)-SC NF membrane.

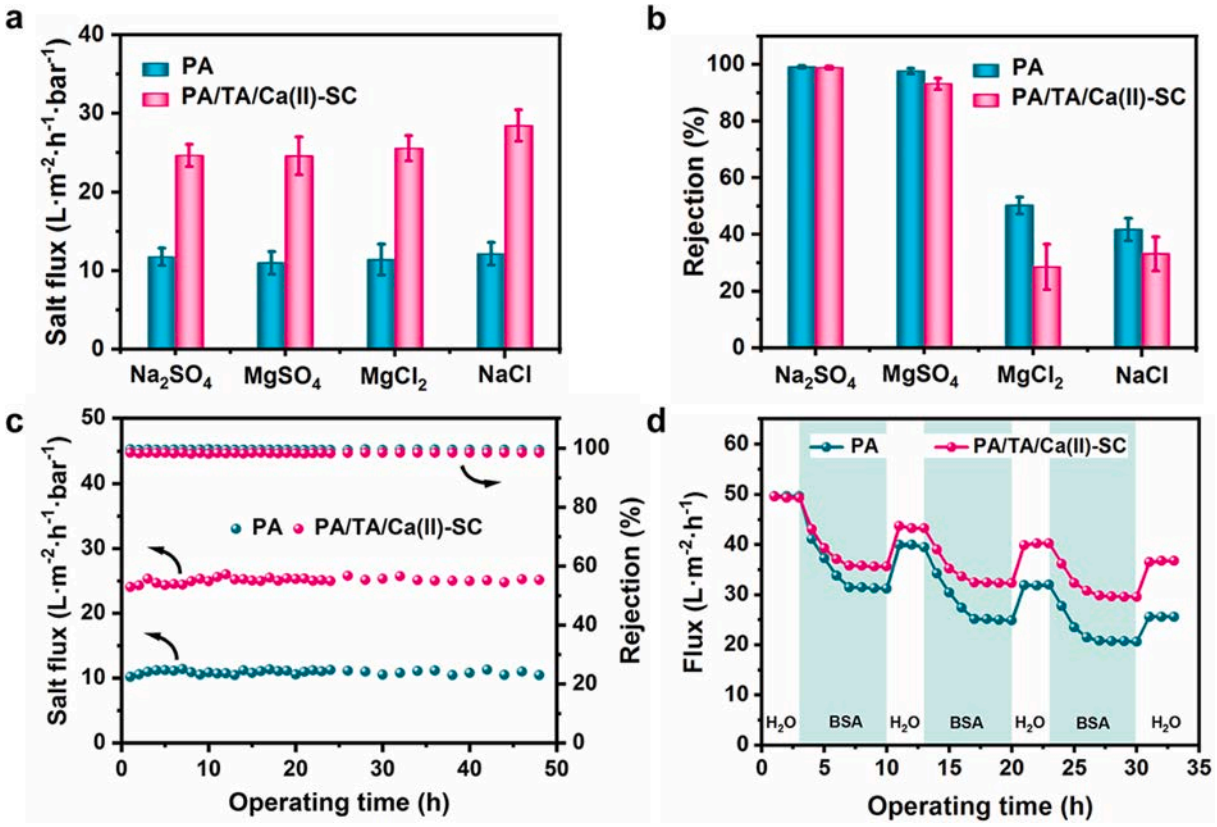

Fig. 7. (a-b) Salt flux and salt rejection of PA and PA/TA/Ca(II)-SC NF membranes. (c) Stability performance of PA and PA/TA/Ca(II)-SC NF membranes tested with Na_2SO_4 solution (1000 ppm) for 48 h at 5 bar. (d) Antifouling performance of PA and PA/TA/Ca(II)-SC NF membranes tested with pure water and 500 ppm BSA solution, respectively.

determined by the synergistic effect of size sieving and strong Donnan exclusion [64,65]. The detailed explanation is as follows: the mean effective pore radius ($r_p = 0.260$ nm) of PA NF membrane is smaller than that of hydrated salt ions (Mg^{2+}=0.428 nm, SO_4^{2-}=0.379 nm, Na^+=0.358 nm, Cl^-=0.332 nm) [66], and its corresponding geometric standard deviation (σ_p) is 1.233, which means that dehydration behavior is required for hydrated ions to transport across the membrane [67]. Due to steric effect, Mg^{2+} with larger radius of hydrated ions is more difficult to dehydrate through the membrane than Na^+, so the rejection rate of $MgCl_2$ is higher than that of NaCl, indicating that size sieving plays a major role in this process [7]. Meanwhile, for the negatively charged PA NF membrane (-42.4 mV), the rejection rate of $MgSO_4$ is higher than that of $MgCl_2$ due to the strong electrostatic repulsion of SO_4^{2-} [8]. However, for PA/TA/Ca(II)-SC NF membrane, the rejection rate of $MgCl_2$ (28.5 %) is lower than that of NaCl (33.2 %), with larger pores ($r_p = 0.289$ nm, $\sigma p = 1.575$) and more negative charge (-45.9 mV), which makes it more attractive to Mg^{2+} and promotes the passage of $MgCl_2$ and has also been reported in our previous work [54].

In order to compare the stability of PA/TA/Ca(II)-SC and PA NF membrane in the separation process, Na_2SO_4 solution (1000 ppm) was used as the feed solution and the membranes were continuously operated for 48 h at 5 bar (Fig. 7c). It can be found that the salt flux and salt rejection remained stable, performing good operation stability of PA/TA/Ca(II)-SC NF membrane. In addition, the PA/TA/Ca(II)-SC NF membrane still showed excellent separation performance when the pH range of feed solution was 5–9 (Fig. S11).

Furthermore, the repeatability of membranes, as one of the most important parameters determining economic viability, was also evaluated in Fig. S12. After five cycles, the pure water flux of PA/TA/Ca(II)-SC NF membrane was still up to 150 $L{\cdot}m^{-2}{\cdot}h^{-1}$ while the Na_2SO_4 rejection rate remained above 98 % at a pressure of 5 bar, showing good repeatability. Subsequently, it can be inferred that the separation layer outside the hollow structure was depressed during the filtration process according to the circle structure on the surface of PA/TA/Ca(II)-SC NF membrane (Fig. S13), but this behavior did not destroy the separation effect based on the separation performance of the membrane. Moreover, the antifouling performance of PA/TA/Ca(II)-SC and PA NF membrane tested with deionized water and 500 ppm BSA solution at 5 bar, respectively (Fig. 7d). After 3.5 cycles, the PA/TA/Ca(II)-SC NF membrane showed higher FRR (91.6 %) and lower FDR (25.9 %) than that of PA NF membrane (Fig. S14). These results demonstrated that the anchoring of SC molecules can enhance the antifouling performance of PA/TA/Ca(II)-SC NF membrane and reduce the attachment of pollutants by improving the hydrophilicity of the membrane surface [43].

We also compared the separation performance of the PA/TA/Ca(II)-SC NF membrane, commercial NF membranes and other surface modified PA-based NF membranes reported in the literature as shown in Fig. 8a and Table S1. Apparently, the PA/TA/Ca(II)-SC NF membrane designed by this CDRIP strategy displays remarkable advantages in terms of permeability and selectivity. Moreover, we explored the influence of SC on the structure and separation performance of PA/TA NF membrane in Fig. S15 and Fig. S16, and further verified that SC mainly improves the membrane permeability by dissociating TA/Ca(II) complex in the preparation of PA/TA/Ca(II)-SC NF membrane. Finally, we summarized the interaction of TA, Ca^{2+} and SC, during complexation and dissociation processes, as well as the regulation of the structure and surface properties of PA-based NF membrane, as shown in Fig. 8b. The synergistic effect of reducing mass transfer resistance and improving surface properties enhances membrane separation performance, and is dedicated to the tailored design of high permeability NF membranes.

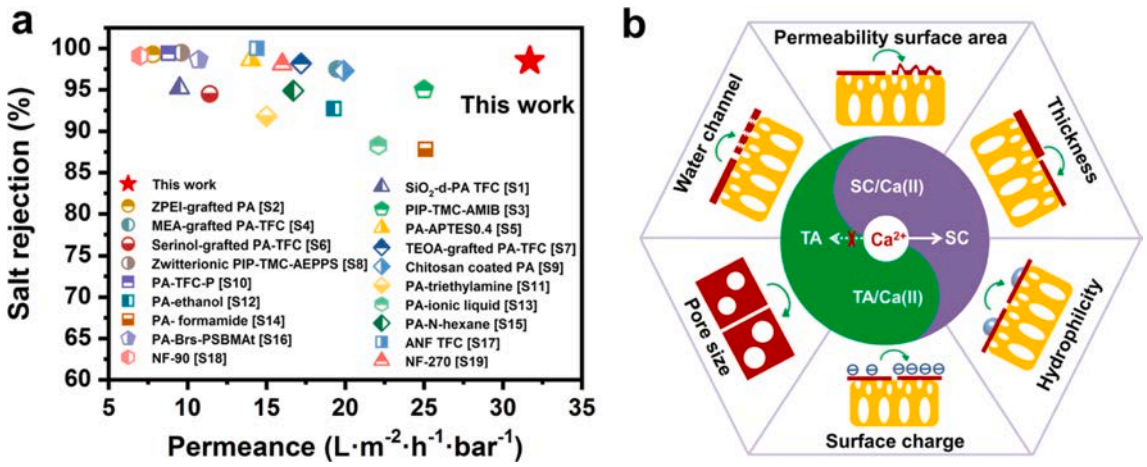

Fig. 8. (a) Comparison of the filtration performance of the PA/TA/Ca(II)-SC NF membrane with commercial NF and other NF membranes reported in the literature. (b) The structure and surface properties of PA-based NF membrane regulated by the interaction of TA, Ca^{2+} and SC.

4. Conclusions

In this work, we developed a green and efficient CDRIP strategy to prepare highly permeable NF membranes by *in situ* forming TA/Ca(II) complexes on substrate surfaces and dissociating them by SC after interfacial polymerization. SC anchored on the surface of PA membrane as well as formed water-soluble SC/Ca(II) complexes to release Ca^{2+} from PA/TA/Ca(II)-SC NF membrane. Additionally, TA remained on the membrane surface after the dissociation of TA/Ca(II) complex, thereby further enhancing hydrophilicity and surface negative charge. The optimal PA/TA/Ca(II)-SC NF membrane was prepared after being soaked in 1 wt% SC solution for 6 h when the Ca^{2+} content was 0.05 wt %. As a result, the PA/TA/Ca(II)-SC NF membrane exhibited a high Na_2SO_4 rejection (98.5 %) and an outstanding water permeability of 31.7 $L{\cdot}m^{-2}{\cdot}h^{-1}{\cdot}bar^{-1}$, which was 2-fold that of the pristine PA NF membrane. It also possessed remarkable advantages in terms of permeability and selectivity compared with commercial NF membranes and the other surface modified PA-based NF membranes published in the literature. The excellent separation performance of this NF membrane can be explained by the synergistic effect of the reduced mass transfer resistance and improved surface properties of the PA layer. Moreover, the PA/TA/Ca(II)-SC NF membrane maintained good operation stability and anti-fouling performance. This study paves a promising strategy to fabricate high-permeability PA-based NF membranes.

Declaration of Competing Interest

The authors declare that they have no known competing financial interests or personal relationships that could have appeared to influence the work reported in this paper.

Data availability

No data was used for the research described in the article.

Acknowledgements

This research was funded by National Key R&D Program of China (No. 2017YFB0602702-02), and thanks eceshi (www.eceshi.com) for the XPS test.

Appendix A. Supplementary data

Supplementary data to this article can be found online at https://doi.org/10.1016/j.cej.2022.139197.

References

[1] L.E. Peng, Z. Yang, L. Long, S. Zhou, H. Guo, C.Y. Tang, A critical review on porous substrates of TFC polyamide membranes: Mechanisms, membrane performances, and future perspectives, J. Membr. Sci. 641 (2022), 119871, https://doi.org/10.1016/j.memsci.2021.119871.
[2] M. Kumar H.A. Stone Membrane science emerging as a convergent scientific field with molecular origins and understanding, and global impact Proc. Natl. Acad. Sci. 118 37 2021 10.1073/pnas.2106494118 e2106494118.
[3] K. Wang, X. Wang, B. Januszewski, Y. Liu, D. Li, R. Fu, M. Elimelech, X. Huang, Tailored design of nanofiltration membranes for water treatment based on synthesis–property–performance relationships, Chem. Soc. Rev. 51 (2) (2022) 672–719.
[4] B. Venkata Swamy M. Madhumala R.S. Prakasham S. Sridhar Nanofiltration of bulk drug industrial effluent using indigenously developed functionalized polyamide membrane Chem. Eng. J. 233 (2013) 193 200 10.1016/j.cej.2013.08.045.
[5] W.H. Organization. Guidelines for Drinking-water Quality, Fourth Edition, World Health Organization. (2011).
[6] M.S.H. Bader, Sulfate scale problems in oil fields water injection operations, Desalination 201 (1) (2006) 100–105, https://doi.org/10.1016/j.desal.2005.09.039.
[7] B. He, H. Peng, Y. Chen, Q. Zhao, High performance polyamide nanofiltration membranes enabled by surface modification of imidazolium ionic liquid, J. Membr. Sci. 608 (2020), 118202, https://doi.org/10.1016/j.memsci.2020.118202.
[8] M. Zhang, X. You, K. Xiao, Z. Yin, J. Yuan, J. Zhao, C. Yang, R. Zhang, H. Wu, Z. Jiang, Modulating interfacial polymerization with phytate as aqueous-phase additive for highly-permselective nanofiltration membranes, J. Membr. Sci. 657 (2022), 120673, https://doi.org/10.1016/j.memsci.2022.120673.
[9] Z.-M. Zhan, Y.-J. Tang, K.-K. Zhu, S.-M. Xue, C.-H. Ji, C.Y. Tang, Z.-L. Xu, Coupling heat curing and surface modification for the fabrication of high permselectivity polyamide nanofiltration membranes, J. Membr. Sci. 623 (2021), 119073, https://doi.org/10.1016/j.memsci.2021.119073.
[10] L. Deng, S. Li, Y. Qin, L. Zhang, H. Chen, Z. Chang, Y. Hu, Fabrication of antifouling thin-film composite nanofiltration membrane via surface grafting of polyethyleneimine followed by zwitterionic modification, J. Membr. Sci. 619 (2021), 118564, https://doi.org/10.1016/j.memsci.2020.118564.
[11] J. Wang, W. Yu, N.J.D. Graham, L. Jiang, Evaluation of a novel polyamide-polyethylenimine nanofiltration membrane for wastewater treatment: Removal of Cu^{2+} ions, Chem. Eng. J. 392 (2020), 123769, https://doi.org/10.1016/j.cej.2019.123769.
[12] H.-F. Xiao, C.-H. Chu, W.-T. Xu, B.-Z. Chen, X.-H. Ju, W. Xing, S.-P. Sun, Amphibian-inspired amino acid ionic liquid functionalized nanofiltration membranes with high water permeability and ion selectivity for pigment wastewater treatment, J. Membr. Sci. 586 (2019) 44–52, https://doi.org/10.1016/j.memsci.2019.05.038.
[13] R. Zhang, S. Yu, W. Shi, X. Wang, J. Cheng, Z. Zhang, L. Li, X. Bao, B. Zhang, Surface modification of piperazine-based nanofiltration membranes with serinol for enhanced antifouling properties in polymer flooding produced water treatment, Rsc Adv. 7 (77) (2017) 48904–48912, https://doi.org/10.1039/C7RA09496E.
[14] F. Yan, H. Chen, Y. Lü, Z. Lü, S. Yu, M. Liu, C. Gao, Improving the water permeability and antifouling property of thin-film composite polyamide nanofiltration membrane by modifying the active layer with triethanolamine, J. Membr. Sci. 513 (2016) 108–116, https://doi.org/10.1016/j.memsci.2016.04.049.
[15] M. Yi, C.H. Lau, S. Xiong, W. Wei, R. Liao, L. Shen, A. Lu, Y. Wang, Zwitterion–Ag Complexes That Simultaneously Enhance Biofouling Resistance and Silver Binding Capability of Thin Film Composite Membranes, ACS Appl. Mater. Interfaces 11 (17) (2019) 15698–15708, https://doi.org/10.1021/acsami.9b02983.

[16] Y.-S. Guo, X.-D. Weng, B. Wu, Y.-F. Mi, B.-K. Zhu, Y.-L. Ji, Q.-F. An, C.-J. Gao, Construction of nonfouling nanofiltration membrane via introducing uniformly tunable zwitterionic layer, J. Membr. Sci. 583 (2019) 152–162, https://doi.org/10.1016/j.memsci.2019.04.055.
[17] S. Karan, Z.W. Jiang, A.G. Livingston, Sub-10 nm polyamide nanofilms with ultrafast solvent transport for molecular separation, Science 348 (6241) (2015) 1347–1351, https://doi.org/10.1126/science.aaa5058.
[18] Y. Hao, Q. Li, B. He, B. Liao, X. Li, M. Hu, Y. Ji, Z. Cui, M. Younas, J. Li, An ultrahighly permeable-selective nanofiltration membrane mediated by an in situ formed interlayer, J Mater Chem A 8 (10) (2020) 5275–5283, https://doi.org/10.1039/C9TA12258C.
[19] Y.-L. Ji, B.-X. Gu, S.-J. Xie, M.-J. Yin, W.-J. Qian, Q. Zhao, W.-S. Hung, K.-R. Lee, Y. Zhou, Q.-F. An, C.-J. Gao, Superfast Water Transport Zwitterionic Polymeric Nanofluidic Membrane Reinforced by Metal–Organic Frameworks, Adv. Mater. 33 (38) (2021) 2102292.
[20] Y. Lin, Q. Shen, Y. Kawabata, J. Segawa, X. Cao, K. Guan, T. Istirokhatun, T. Yoshioka, H. Matsuyama, Graphene quantum dots (GQDs)-assembled membranes with intrinsic functionalized nanochannels for high-performance nanofiltration, Chem. Eng. J. 420 (2021), 127602, https://doi.org/10.1016/j.cej.2020.127602.
[21] Y. Lu R. Wang Y. Zhu Z. Wang W. Fang S. Lin J. Jin Two-dimensional fractal nanocrystals templating for substantial performance enhancement of polyamide nanofiltration membrane Proc. Natl. Acad. Sci. 118 37 2021 10.1073/pnas.2019891118 e2019891118.
[22] Z. Tan, S.F. Chen, X.S. Peng, L. Zhang, C.J. Gao, Polyamide membranes with nanoscale Turing structures for water purification, Science 360 (6388) (2018) 518-+, https://doi.org/10.1126/science.aar6308.
[23] N. Zhang, X. Song, H. Jiang, C.Y. Tang, Advanced thin-film nanocomposite membranes embedded with organic-based nanomaterials for water and organic solvent purification: A review, Sep. Purif. Technol. 269 (2021), 118719, https://doi.org/10.1016/j.seppur.2021.118719.
[24] C. Lei, J. Gao, W. Ren, Y. Xie, S.Y.H. Abdalkarim, S. Wang, Q. Ni, J. Yao, Fabrication of metal-organic frameworks@cellulose aerogels composite materials for removal of heavy metal ions in water, Carbohydr. Polym. 205 (2019) 35–41, https://doi.org/10.1016/j.carbpol.2018.10.029.
[25] R.M. Rego, M.D. Kurkuri, M. Kigga, A comprehensive review on water remediation using UiO-66 MOFs and their derivatives, Chemosphere 302 (2022), 134845, https://doi.org/10.1016/j.chemosphere.2022.134845.
[26] P. Chen, X. Ma, Z. Zhong, F. Zhang, W. Xing, Y. Fan, Performance of ceramic nanofiltration membrane for desalination of dye solutions containing NaCl and Na_2SO_4, Desalination 404 (2017) 102–111, https://doi.org/10.1016/j.desal.2016.11.014.
[27] Z. Yang, X.-H. Ma, C.Y. Tang, Recent development of novel membranes for desalination, Desalination 434 (2018) 37–59, https://doi.org/10.1016/j.desal.2017.11.046.
[28] M. Chen, X. Qin, G. Zeng, Biodegradation of Carbon Nanotubes, Graphene, and Their Derivatives, Trends Biotechnol. 35 (9) (2017) 836–846, https://doi.org/10.1016/j.tibtech.2016.12.001.
[29] H.J. Kim, D.-G. Kim, H. Yoon, Y.-S. Choi, J. Yoon, J.-C. Lee, Polyphenol/FeIII Complex Coated Membranes Having Multifunctional Properties Prepared by a One-Step Fast Assembly, Adv. Mater. Interfaces. 2 (14) (2015) 1500298, https://doi.org/10.1002/admi.201500298.
[30] F. You, Y. Xu, X. Yang, Y. Zhang, L.u. Shao, Bio-inspired Ni 2+ -polyphenol hydrophilic network to achieve unconventional high-flux nanofiltration membranes for environmental remediation, Chem. Commun. 53 (45) (2017) 6128–6131.
[31] Y. Zhou X. Wu J. Zhang Z. Wang In situ formation of tannic (TA)-aminopropyltriethoxysilane (APTES) nanospheres on inner and outer surface of polypropylene membrane toward enhanced dye removal capacity Chem. Eng. J. 433 2022 133843 10.1016/j.cej.2021.133843.
[32] G.H. Liu, Z.Y. Jiang, C. Chen, L.P. Hou, B.X. Gao, H. Yang, H. Wu, F.S. Pan, P. Zhang, X.Z. Cao, Preparation of ultrathin, robust membranes through reactive layer-by-layer (LbL) assembly for pervaporation dehydration, J. Membr. Sci. 537 (2017) 229–238, https://doi.org/10.1016/j.memsci.2017.05.025.
[33] S. Guo, H. Zhang, X. Chen, S. Feng, Y. Wan, J. Luo, Fabrication of Antiswelling Loose Nanofiltration Membranes via a "Selective-Etching-Induced Reinforcing" Strategy for Bioseparation, ACS Appl. Mater. Interfaces 13 (16) (2021) 19312–19323, https://doi.org/10.1021/acsami.1c02611.
[34] J.L. Meyer, Formation constants for interaction of citrate with calcium and magnesium ions, Anal. Biochem. 62 (1) (1974) 295–300, https://doi.org/10.1016/0003-2697(74)90391-1.
[35] X. Dong, Q.-W. Meng, W. Hu, R. Chen, Q. Ge, Forward osmosis membrane developed from the chelation of Fe^{3+} and carboxylate for trace organic contaminants removal, Chem. Eng. J. 428 (2022), 131091, https://doi.org/10.1016/j.cej.2021.131091.
[36] L. Yu, K. Li, Y. Zhang, J. Wang, G. Zhang, Improved permeability of tight acid resistant nanofiltration membrane via citric acid post-treatment, J. Membr. Sci. 648 (2022), 120381, https://doi.org/10.1016/j.memsci.2022.120381.
[37] N. Zhang, Z. Huang, N. Yang, L. Zhang, B. Jiang, Y. Sun, J. Ma, Nanofiltration membrane via EGCG-PEI co-deposition followed by cross-linking on microporous PTFE substrates for desalination, Sep. Purif. Technol. 232 (2020), 115964, https://doi.org/10.1016/j.seppur.2019.115964.
[38] J. Lin, W. Ye, M.-C. Baltaru, Y.P. Tang, N.J. Bernstein, P. Gao, S. Balta, M. Vlad, A. Volodin, A. Sotto, P. Luis, A.L. Zydney, B. Van der Bruggen, Tight ultrafiltration membranes for enhanced separation of dyes and Na_2SO_4 during textile wastewater treatment, J. Membr. Sci. 514 (2016) 217–228, https://doi.org/10.1016/j.memsci.2016.04.057.
[39] A.S. Michaels, Analysis and Prediction of Sieving Curves for Ultrafiltration Membranes: A Universal Correlation? Sep. Sci. Technol. 15 (6) (1980) 1305–1322, https://doi.org/10.1080/01496398008068507.
[40] Y. Chen, Y. Bai, L. Meng, W. Zhang, J. Xia, Z. Xu, R. Sun, Y. Lv, T. Liu, Engineering nanocomposite metal-phenolic network membranes with hollow MOFs via in-situ etching for High-efficiency organic solvent nanofiltration, Chem. Eng. J. 437 (2022), 135289, https://doi.org/10.1016/j.cej.2022.135289.
[41] S. Li, B. Gao, Y. Wang, B. Jin, Q. Yue, Z. Wang, Antibacterial thin film nanocomposite reverse osmosis membrane by doping silver phosphate loaded graphene oxide quantum dots in polyamide layer, Desalination 464 (2019) 94–104, https://doi.org/10.1016/j.desal.2019.04.029.
[42] D. Wang, J. Li, B. Gao, Y. Chen, Z. Wang, Triple-layered thin film nanocomposite membrane toward enhanced forward osmosis performance, J. Membr. Sci. 620 (2021), 118879, https://doi.org/10.1016/j.memsci.2020.118879.
[43] J. Zheng, R. Zhao, A.A. Uliana, Y. Liu, D. de Donnea, X. Zhang, D. Xu, Q. Gao, P. Jin, Y. Liu, A. Volodine, J. Zhu, B. Van der Bruggen, Separation of textile wastewater using a highly permeable resveratrol-based loose nanofiltration membrane with excellent anti-fouling performance, Chem. Eng. J. 434 (2022), 134705, https://doi.org/10.1016/j.cej.2022.134705.
[44] J. Zhao, Q. Wang, J. Yang, Y. Li, Z. Liu, L. Zhang, Y. Zhao, S. Zhang, L. Chen, Comb-shaped amphiphilic triblock copolymers blend PVDF membranes overcome the permeability-selectivity trade-off for protein separation, Sep. Purif. Technol. 239 (2020), 116596, https://doi.org/10.1016/j.seppur.2020.116596.
[45] D. Wang, D. Li, Y. Liu, D. Lv, Y. Ye, S. Zhu, B. Zhang, Study of a new complex method for extraction of phenolic compounds from bio-oils, Sep. Purif. Technol. 134 (2014) 132–138, https://doi.org/10.1016/j.seppur.2014.07.033.
[46] M. Leopoldini, N. Russo, S. Chiodo, M. Toscano, Iron Chelation by the Powerful Antioxidant Flavonoid Quercetin, J. Agric. Food Chem. 54 (17) (2006) 6343–6351, https://doi.org/10.1021/jf060986h.
[47] M. Leopoldini, N. Russo, M. Toscano, The molecular basis of working mechanism of natural polyphenolic antioxidants, Food Chem. 125 (2) (2011) 288–306, https://doi.org/10.1016/j.foodchem.2010.08.012.
[48] D.-B. Li, Y.-Q. Liu, Y.-Y. Ye, S.-R. Li, D. Wang, Study of reaction mechanism between guaiacol and $Ca(OH)_2$ in water: Development of a novel phenol extraction method, J. Cleaner Prod. 172 (2018) 2853–2861, https://doi.org/10.1016/j.jclepro.2017.11.128.
[49] S. Hao, K. Chen, L. Cao, X. Zhu, G. Luo, S. Zhang, J. Chen, Separation of high-purity syringol and acetosyringone from rice straw-derived bio-oil by combining the basification-acidification process and column chromatography, Electrophoresis 37 (19) (2016) 2522–2530, https://doi.org/10.1002/elps.201600126.
[50] X. Zhang, P.-F. Ren, H.-C. Yang, L.-S. Wan, Z.-K. Xu, Co-deposition of tannic acid and diethlyenetriamine for surface hydrophilization of hydrophobic polymer membranes, Appl. Surf. Sci. 360 (2016) 291–297, https://doi.org/10.1016/j.apsusc.2015.11.015.
[51] Q. Guo, X. Wu, Y. Ji, Y. Hao, S. Liao, Z. Cui, J. Li, M. Younas, B. He, pH-responsive nanofiltration membrane containing chitosan for dye separation, J. Membr. Sci. 635 (2021), 119445, https://doi.org/10.1016/j.memsci.2021.119445.
[52] H. Peng, W.-H. Zhang, W.-S. Hung, N. Wang, J. Sun, K.-R. Lee, Q.-F. An, C.-M. Liu, Q. Zhao, Phosphonium Modification Leads to Ultrapermeable Antibacterial Polyamide Composite Membranes with Unreduced Thickness, Adv. Mater. 32 (23) (2020) 2001383, https://doi.org/10.1002/adma.202001383.
[53] Y.-L. Liu, Y.-Y. Zhao, X.-M. Wang, X.-H. Wen, X. Huang, Y.F. Xie, Effect of varying piperazine concentration and post-modification on prepared nanofiltration membranes in selectively rejecting organic micropollutants and salts, J. Membr. Sci. 582 (2019) 274–283, https://doi.org/10.1016/j.memsci.2019.04.018.
[54] N. Zhang, X.J. Song, Y.Q. Chen, B. Jiang, L.H. Zhang, H.Q. Jiang, A facile and economic route assisted by trace tannic acid to construct a high-performance thin film composite NF membrane for desalination, Environ. Sci. Water Res. Technol. 7 (5) (2021) 956–968, https://doi.org/10.1039/d1ew00071c.
[55] Q. Yao, S. Li, R. Zhang, L. Han, B. Su, High-throughput thin-film composite membrane via interfacial polymerization using monomers of ultra-low concentration on tannic acid – Copper interlayer for organic solvent nanofiltration, Sep. Purif. Technol. 258 (2021), 118027, https://doi.org/10.1016/j.seppur.2020.118027.
[56] X. Zhang, Y. Lv, H.-C. Yang, Y. Du, Z.-K. Xu, Polyphenol Coating as an Interlayer for Thin-Film Composite Membranes with Enhanced Nanofiltration Performance, ACS Appl. Mater. Interfaces 8 (47) (2016) 32512–32519, https://doi.org/10.1021/acsami.6b10693.
[57] Q. Li, Z. Liao, X. Fang, J. Xie, L. Ni, D. Wang, J. Qi, X. Sun, L. Wang, J. Li, Tannic acid assisted interfacial polymerization based loose thin-film composite NF membrane for dye/salt separation, Desalination 479 (2020), 114343, https://doi.org/10.1016/j.desal.2020.114343.
[58] X.H. Ma, Z.K. Yao, Z. Yang, H. Guo, Z.L. Xu, C.Y. Tang, M. Elimelech, Nanofoaming of Polyamide Desalination Membranes To Tune Permeability and Selectivity, Environ. Sci. Technol. Lett. 5 (2) (2018) 123–130, https://doi.org/10.1021/acs.estlett.8b00016.
[59] R. Zhang, M. He, D. Gao, Y. Liu, M. Wu, Z. Jiao, Y. Su, Z. Jiang, Polyphenol-assisted in-situ assembly for antifouling thin-film composite nanofiltration membranes, J. Membr. Sci. 566 (2018) 258–267, https://doi.org/10.1016/j.memsci.2018.09.010.
[60] S. Wang, Q. Li, B. He, M. Gao, Y. Ji, Z. Cui, F. Yan, X. Ma, M. Younas, J. Li, Preparation of Small-Pore Ultrafiltration Membranes with High Surface Porosity by In Situ CO2 Nanobubble-Assisted NIPS, ACS Appl. Mater. Interfaces 14 (6) (2022) 8633–8643, https://doi.org/10.1021/acsami.1c23760.

[61] W.-X. Li, Z. Yang, W.-L. Liu, Z.-H. Huang, H. Zhang, M.-P. Li, X.-H. Ma, C.Y. Tang, Z.-L. Xu, Polyamide reverse osmosis membranes containing 1D nanochannels for enhanced water purification, J. Membr. Sci. 618 (2021) 118681.
[62] X. Fan, Y. Dong, Y. Su, X. Zhao, Y. Li, J. Liu, Z. Jiang, Improved performance of composite nanofiltration membranes by adding calcium chloride in aqueous phase during interfacial polymerization process, J. Membr. Sci. 452 (2014) 90–96, https://doi.org/10.1016/j.memsci.2013.10.026.
[63] BeiBei Tang, C. Zou, P. Wu, Study on a novel polyester composite nanofiltration membrane by interfacial polymerization. II. The role of lithium bromide in the performance and formation of composite membrane, Journal of Membrane Science 365 (1-2) (2010) 276–285.
[64] L. Zhang, R. Zhang, M. Ji, Y. Lu, Y. Zhu, J. Jin, Polyamide nanofiltration membrane with high mono/divalent salt selectivity via pre-diffusion interfacial polymerization, J. Membr. Sci. 636 (2021), 119478, https://doi.org/10.1016/j.memsci.2021.119478.
[65] Y. Liang, Y. Zhu, C. Liu, K.-R. Lee, W.-S. Hung, Z. Wang, Y. Li, M. Elimelech, J. Jin, S. Lin, Polyamide nanofiltration membrane with highly uniform sub-nanometre pores for sub-1 Å precision separation, Nat. Commun. 11 (1) (2020) 2015, https://doi.org/10.1038/s41467-020-15771-2.
[66] Y. Li, E. Wong, Z. Mai, B. Van der Bruggen, Fabrication of composite polyamide/Kevlar aramid nanofiber nanofiltration membranes with high permselectivity in water desalination, J. Membr. Sci. 592 (2019), 117396, https://doi.org/10.1016/j.memsci.2019.117396.
[67] C. Lu, C. Hu, C.L. Ritt, X. Hua, J. Sun, H. Xia, Y. Liu, D.-W. Li, B. Ma, M. Elimelech, J. Qu, In Situ Characterization of Dehydration during Ion Transport in Polymeric Nanochannels, J. Am. Chem. Soc. 143 (35) (2021) 14242–14252, https://doi.org/10.1021/jacs.1c05765.